



# The performance of $\text{La}_{0.6}\text{Sr}_{1.4}\text{MnO}_4$ layered perovskite electrode material for intermediate temperature symmetrical solid oxide fuel cells

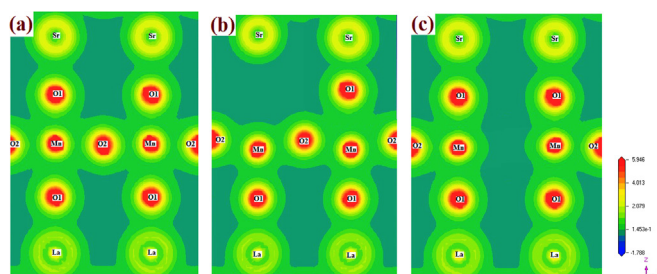
Jun Zhou, Gang Chen\*, Kai Wu\*, Yonghong Cheng

State Key Laboratory of Electrical Insulation and Power Equipment, Xi'an Jiaotong University, Xi'an 710049, People's Republic of China

## HIGHLIGHTS

- Conductivities of  $\text{LSMO}_4$  in air and 5%  $\text{H}_2$  were  $5.5$  and  $0.4 \times 10^{-2} \text{ S cm}^{-1}$  at  $800^\circ\text{C}$ .
- DFT +  $U$  calculations show oxygen vacancies block the 3D hopping path for carriers.
- The single cell shows a maximum cell power density of  $59 \text{ mW cm}^{-2}$  at  $800^\circ\text{C}$ .

## GRAPHICAL ABSTRACT



## ARTICLE INFO

### Article history:

Received 15 March 2014

Received in revised form

25 April 2014

Accepted 30 June 2014

Available online 15 July 2014

### Keywords:

Symmetrical solid oxide fuel cells

Electrode materials

Mixed ionic–electronic conductor

Density functional theory

## ABSTRACT

A layered perovskite electrode material,  $\text{La}_{0.6}\text{Sr}_{1.4}\text{MnO}_{4+\delta}$  ( $\text{LSMO}_4$ ), has been studied for intermediate temperature symmetrical solid oxide fuel cells (IT-SOFCs) on  $\text{La}_{0.9}\text{Sr}_{0.1}\text{Ga}_{0.8}\text{Mg}_{0.2}\text{O}_{3-\delta}$  (LSGM) electrolyte. The chemical compatibility tests indicate that no reaction occurred between  $\text{LSMO}_4$  oxide and LSGM electrolyte at temperature up to  $1000^\circ\text{C}$  both in air and 5%  $\text{H}_2$ . The lower conductivity in 5%  $\text{H}_2$  and higher conduction activation energy than those in air would be caused by poorer overlap of both  $\sigma$  and  $\pi$  bonds. DFT +  $U$  calculations also show that oxygen vacancies which formed in reducing atmosphere may block the 3D hopping path for electrons or holes through Mn–O–Mn chains. For  $\text{LSMO}_4$  electrode, SEM results indicate that the electrode formed good contact with the electrolyte after being sintered at  $900^\circ\text{C}$  for 2 h. At  $800^\circ\text{C}$ , the polarization resistance of the  $\text{LSMO}_4$  cathode is about  $0.87 \Omega \text{ cm}^2$  in air, while the polarization resistance of the  $\text{LSMO}_4$  anode is about  $2.07 \Omega \text{ cm}^2$  in 5%  $\text{H}_2$ .  $\text{LSMO}_4$  exhibits better electrochemical activity for oxygen reduction than that for hydrogen oxidation. A cell with LSGM electrolyte,  $\text{LSMO}_4$ –LSGM mixture as anode and cathode simultaneously displays a maximum power density of  $59 \text{ mW cm}^{-2}$  at  $800^\circ\text{C}$ .

© 2014 Elsevier B.V. All rights reserved.

## 1. Introduction

The solid oxide fuel cell (SOFC) technology has experienced a substantial interest in recent years due to its higher efficiency and

\* Corresponding authors. Tel./fax: +86 029 82664480.

E-mail addresses: [zhoujun@mail.xjtu.edu.cn](mailto:zhoujun@mail.xjtu.edu.cn) (J. Zhou), [chainway@mail.xjtu.edu.cn](mailto:chainway@mail.xjtu.edu.cn) (G. Chen), [wukai@mail.xjtu.edu.cn](mailto:wukai@mail.xjtu.edu.cn) (K. Wu).

lower pollution emissions than these of fossil fuels. A traditional high temperature SOFC is designed as a sandwich structure of cathode/electrolyte/anode, in which porous electrodes are separated by a dense electrolyte [1]. Since the gases reach each electrode compartment separately, both materials must fulfil some general requirements: stability of the microstructure during the preparation and operation processes in a single cell; chemical stability and thermal expansion coefficients (TECs) closer to those of the other cell components; and adequate porosity and catalytic

activity to achieve the highest performances [2]. Moreover, cathode and anode must show proper electronic conductivity and stability in oxidising and reducing conditions, respectively. However, a big shortcoming is the high operating temperatures (900–1000 °C), which caused the components degradation and the high fabrication and operating costs [3]. Reducing the operating temperature with sufficient power output and durability appears to be the challenge of intermediate temperature solid oxide fuel cells (IT-SOFCs, operating temperature: 600–800 °C) [4]. Especially, a major problem is the increased polarization resistance of the electrode at lower operating temperatures [5]. Thus, it is important to develop new electrode materials with good electrochemical properties at low operation temperatures.

The traditional SOFC configuration may be replaced by a new strategy, where the same electrode material could be used simultaneously as both anode and cathode to build a symmetrical Solid Oxide Fuel Cell (SSOFC) [6]. Bastidas et al. first reported that the  $\text{La}_{0.75}\text{Sr}_{0.25}\text{Cr}_{0.5}\text{Mn}_{0.5}\text{O}_3$  (LSCM) compound can apply as symmetrical electrode for a LSCM/YSZ/LSCM fuel cell, and maximum power densities of  $300 \text{ mW cm}^{-2}$  and  $230 \text{ mW cm}^{-2}$  were obtained using wet  $\text{H}_2$  and wet  $\text{CH}_4$  at 900 °C [7]. Then, several excellent studies focused on perovskite related materials [8–15] and some electrodes show reasonable performance. For example, Pena-Martinez et al. [8] tested several potential symmetrical materials  $\text{La}_{0.75}\text{Sr}_{0.25}\text{Cr}_{0.5}\text{X}_{0.5}\text{O}_{3-d}$ ,  $\text{X} = \text{Mn, Fe and Al}$ , (LSCrM, LSCrF and LSCrA) with LSGM electrolyte. The study showed that the maximum power density ( $123 \text{ mW cm}^{-2}$ ) at 800 °C was reached with the electrolyte-supported system BSCoF/LSGM/LSCrM. Zhang et al. [9] reported a composite symmetrical electrode,  $\text{La}_{0.7}\text{Ca}_{0.3}\text{CrO}_{3-\delta}-\text{Ce}_{1-x}\text{Gd}_x\text{O}_{2-\delta}$ . The performances obtained in a fuel cell were 387 and  $573 \text{ mW cm}^{-2}$  at 850 and 900 °C respectively, under dry  $\text{H}_2$  using a 300  $\mu\text{m}$  layer of LSGM as electrolyte. El-Himri et al. [15] studied a new series of compound as symmetrical electrode based on  $\text{Pr}_{0.7}\text{Ca}_{0.3}\text{Cr}_{1-y}\text{Mn}_y\text{O}_{3-d}$  ( $y = 0.2-0.8$ ). An assembled SSOFC rendered performances of 250 and  $160 \text{ mW cm}^{-2}$  at 950 °C under humidified  $\text{H}_2$  and  $\text{CH}_4$  respectively. In addition, Liu Q. et al. reported that  $\text{Sr}_2\text{Fe}_{1.5}\text{Mo}_{0.5}\text{O}_{6-\delta}$ , exhibiting excellent redox stability and remarkable electrical conductivity, is a good candidate electrode for SSFOCs [16].

As we know, the electrode (anode and cathode) should possess several properties including high-catalytic activity for fuel oxidation or oxygen reduction, high-electrical conductivity, thermal stability, and compatibility with other cell components in reducing and oxidizing condition respectively. Mixed ionic and electronic conductors (MIECs) are concentrated as good electrode candidates. Recently, a new family of  $\text{Ln}_2\text{MO}_4$  oxides with  $\text{K}_2\text{NiF}_4$  structure has been reported as a type of good mixed ionic electronic conductor (MIEC) materials [17–27]. The ideal  $\text{K}_2\text{NiF}_4$  structure can be regarded as the alternative stacking of perovskite type layers and rock salt type layers. These materials are considered good cathode candidates for SOFCs due to their better thermal stability, smaller thermal expansion coefficients ( $10.5-14.2 \times 10^{-6} \text{ K}^{-1}$ ) [28–30], which match better with those of the commonly used electrolyte, such as YSZ,  $\text{Ce}_{0.9}\text{Gd}_{0.1}\text{O}_{2-\delta}$  (CGO) or  $\text{La}_{0.9}\text{Sr}_{0.1}\text{Ga}_{0.8}\text{Mg}_{0.2}\text{O}_3$  (LSGM). Most of the compounds with  $\text{K}_2\text{NiF}_4$  structure have the ability to accommodate large amount of interstitial oxygen or generate lots of oxygen vacancies. Therefore, large oxygen diffusion values have been evidenced for  $\text{Ln}_2\text{MO}_4$  oxides compared to the perovskite ones [31]. These advantages make  $\text{Ln}_2\text{MO}_4$  as good candidates as cathode for SOFCs. However, due to poor stability and decomposition for most of  $\text{Ln}_2\text{MO}_4$  oxides under reducing condition at high temperature, only  $\text{La}_{0.6}\text{Sr}_{1.4}\text{MnO}_4$  was reported to be a promise anode for SOFCs [32]. Meanwhile,  $\text{La}_{0.6}\text{Sr}_{1.4}\text{MnO}_4$  also was studied for cathode and showed proper performance [19].

In the present work,  $\text{La}_{0.6}\text{Sr}_{1.4}\text{MnO}_4$  (LSMO<sub>4</sub>) layered perovskite oxide was prepared and characterized by XRD, SEM, TEM and TGA, respectively. DFT + *U* calculations were also performed to investigate the different behaviour of conductivity between that in air and reducing atmosphere. The electrochemical properties of LSMO<sub>4</sub> compounds as electrode on LSGM electrolyte for IT-SSOFCs have been investigated in detail.

## 2. Experimental

### 2.1. Sample preparation

The original material of  $\text{La}_{0.6}\text{Sr}_{1.4}\text{MnO}_4$  (LSMO) was prepared with a citric-nitrate process. Stoichiometric quantities of  $\text{La}(\text{NO}_3)_3 \cdot 6\text{H}_2\text{O}$ ,  $\text{Sr}(\text{NO}_3)_2$ , and  $\text{Mn}(\text{NO}_3)_2$  (all in analytical purity) were dissolved in a certain amount of deionized water. Citric acid, in a molar ratio of 4.5:1 to the total metallic ions, was subsequently added to obtain a homogeneous solution. A porous xerogel was formed at 110 °C and then transformed into LSMO<sub>4</sub> black power after calcined at 1100 °C for 4 h in air. Then, the sample was subsequently heated in flowing 5%  $\text{H}_2/\text{Ar}$  gas (at 900 °C for 20 h) in order to evaluate the stability of this material under reducing condition.

The electrolyte  $\text{La}_{0.9}\text{Sr}_{0.1}\text{Ga}_{0.8}\text{Mg}_{0.2}\text{O}_{3-\delta}$  (LSGM) was prepared by solid-state reaction. Appropriate amounts of high-purity  $\text{La}_2\text{O}_3$ ,  $\text{SrCO}_3$ ,  $\text{Ga}_2\text{O}_3$ , and  $\text{MgO}$  were mixed after drying to remove the absorbed water. After mixed thoroughly, the mixture was pressed into a pellet and finally fired at 1500 °C for 10 h in air. A single perovskite phase was formed according to the XRD pattern. Pellets with thickness of 1.1 mm were prepared for electrolyte-supported cell tests.

The half cells were fabricated as follows: mixed slurry was made of LSMO<sub>4</sub> and LSGM (in a weight ratio of 7:3). The mixture was then screen-printed onto both sides of the LSGM pellets followed by calcination at 900 °C for 2 h. Silver paste and silver wires were used for current collection.

The single cell was fabricated on an LSGM pellet. A layer of LSMO<sub>4</sub>–LSGM composite electrode was printed on both sides of the LSGM pellet and fired at 900 °C for 2 h to form 1.2  $\text{cm}^2$  working area. Silver was used as current collectors for both electrodes and the cells were tested in a four-probe configuration.

### 2.2. Characterization

For phase identification and chemical compatibility confirmation, X-ray diffraction (XRD) was performed on Philips Model PW1050 diffractometer operated at 40 kV and 30 mA using  $\text{CuK}\alpha$  radiation, employing  $\text{CuK}\alpha$  radiation at a step of  $0.02^\circ$  in a  $2\theta$  range of  $10^\circ-80^\circ$ . The obtained XRD profile of samples was analyzed by the Rietveld method with the GSAS [33]. Thermogravimetric analyses (TGA) were carried out in order to determine the oxygen stoichiometry changes of the samples. The TGA experiments were conducted on a NETZSCH TG 209 instrument (NETZSCHGerätebau GmbH, Germany). Measurements were carried out on powders in a temperature range of 25–900 °C at a heating/cooling rate of  $5^\circ\text{C min}^{-1}$ . The microstructure of the LSMO<sub>4</sub> electrode was inspected with a JEOL Model JSM 6700F scanning electron microscopy (SEM). Energy dispersive X-ray spectroscopy (EDS) microanalysis using an Oxford Link ISIS system was performed to check the composition of the samples. The SEM/EDX analysis allows quantitative analysis of large grains ( $\sim 1 \mu\text{m}$  and larger). Prepared LSMO<sub>4</sub> powder and reduced sample were inspected by high-resolution transmission electron microscopy (HRTEM), JEOL JEM2011 (JEOL, Tokyo, Japan). In order to measure the electrical conductivity of the electrode, pressed pellet were fired at 1450 °C

for 10 h. Au paste and mesh were applied as current collector. A standard direct current (dc) four terminal method was used in a temperature range of 50–800 °C in air or 5% H<sub>2</sub>/Ar, respectively. The density of the sintered pellet was measured by Archimedes method. The relative density of LSMO<sub>4</sub> is about 87%. The polarization resistance ( $R_p$ ) of the electrode/electrolyte interface as a function of temperature was determined by AC impedance spectroscopy employing the Schlumberger Solartron 1255 frequency response analyser in the range 1 MHz to 0.01 Hz, coupled with a 1287 electrochemical interface and controlled by Z-plot impedance software. The fuel cell tests were performed on a two electrode setup using wet H<sub>2</sub> as fuel at anode and air as oxidant at cathode.

### 2.3. DFT studies

Density functional theory (DFT +  $U$ ) calculations with the  $U = 3.5$  eV correction for Mn 3d electrons were performed with the CASTEP Simulation Package [34,35] and exchange-correlation was treated in the Perdew-Wang-91 generalized gradient approximation [36,37]. Electronic wave functions were expanded in a plane wave basis set, and ionic cores were described by ultrasoft pseudopotentials [38]. A 340 eV plane wave basis set the cutoff, and the cutoff energy was used all of our calculations. La, Sr, Mn, O atoms are described by 11 (5s<sup>2</sup>5p<sup>6</sup>5d<sup>1</sup>6s<sup>2</sup>), 10 (4s<sup>2</sup>4p<sup>6</sup>5s<sup>2</sup>), 7 (3d<sup>5</sup>4s<sup>2</sup>), 6 (2s<sup>2</sup>sp<sup>4</sup>) valence electrons, respectively. A relaxation is performed for the constructed  $2 \times 1 \times 1$  supercell by using BFGS algorithm [39] to minimize the energy with respect to atomic position. The tolerances for self-consistence are set at  $1.0 \times 10^{-6}$  eV atom<sup>-1</sup> for total energy, 0.01 eV Å<sup>-1</sup> for force,  $2.0 \times 10^{-5}$  eV atom<sup>-1</sup> for band energy, 0.1 GPa for maximum stress and 0.005 Å for the maximum displacement. Spin polarized method was used to describe the magnetic structure of LSMO<sub>4</sub>. Due to LSMO<sub>4</sub> exhibit antiferromagnetic (AFM) ordering and charge-orbital ordering [40], we performed all calculations for the AFM configuration. In order to simulate realistic non-stoichiometric LSMO<sub>4</sub>, oxygen vacancies ( $V_O$ ) were introduced by removing a neutral O atom from the supercell.

## 3. Results and discussion

### 3.1. XRD analysis

The refined XRD patterns showed the pre-prepared and the reduced LSMO<sub>4</sub> powders to be single-phase with no excess peaks of starting materials or other impurities (Figs. 1 and 2). Both patterns

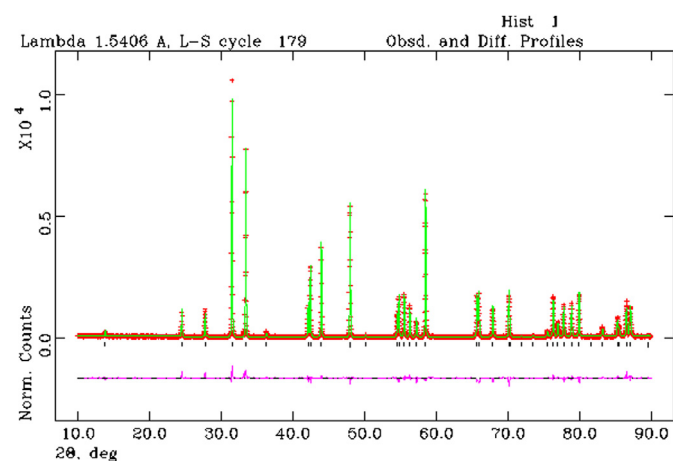


Fig. 1. X-ray diffraction profiles of LSMO<sub>4</sub> formed at 1100 °C, showing observed pattern, peak positions and difference profile.

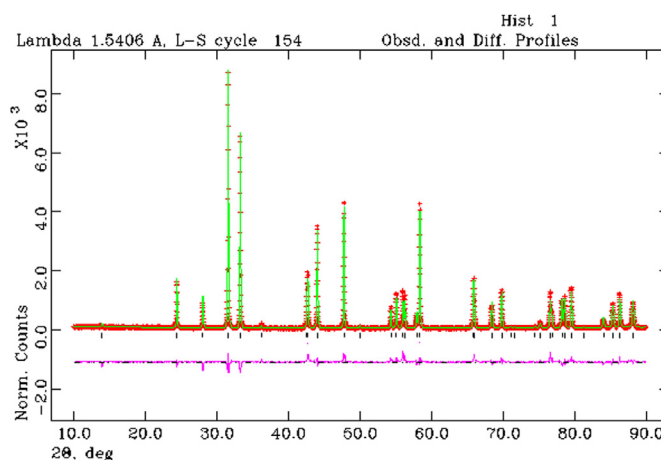


Fig. 2. X-ray diffraction profiles of LSMO<sub>4</sub> after heating at 900 °C in 5% H<sub>2</sub>/Ar for 20 h, showing observed pattern, peak positions and difference profile.

were indexed on a body-centered tetragonal unit cell related to a K<sub>2</sub>NiF<sub>4</sub>-type structure. The XRD pattern of reduced sample shows that LSMO<sub>4</sub> is very stable under reducing atmosphere. Since the refinements of X-ray diffraction were insensitive to oxide ion site occupancy, oxide ion sites and occupancy were therefore fixed. The refined unit cell parameters are given in Table 1 and Table 2. Because the ionic sizes of Mn<sup>4+</sup>, Mn<sup>3+</sup> and Mn<sup>2+</sup> are 0.53, 0.65 and 0.82 Å [41], respectively, the results showed that a slightly increase in unit cell parameters occurs due to the reduction of Mn<sup>4+</sup>/Mn<sup>3+</sup> to Mn<sup>3+</sup>/Mn<sup>2+</sup>. Thus, a larger volume was obtained under reduction as a whole.

Furthermore, for the effective application, the chemical reaction between the electrolyte and electrode is undesirable for the long term stability of SOFCs. The reactivity of LSMO<sub>4</sub> with the LSGM electrolyte was further studied by mixing LSMO<sub>4</sub> and LSGM powders with a 1:1 weight ratio, and sintered in air and 5% H<sub>2</sub> at 900 °C for 10 h, respectively. Fig. 3 shows the XRD patterns of LSMO<sub>4</sub>, LSGM, and the LSMO<sub>4</sub>–LSGM mixture. It clearly exhibits that the main peaks of LSMO<sub>4</sub> and LSGM were present and no other secondary phases were obtained, indicating that LSMO<sub>4</sub> is chemical compatibility with LSGM both in air and 5% H<sub>2</sub> (see Table 3).

### 3.2. TGA

Fig. 4 shows the thermogravimetric programmed reduction of prepared LSMO<sub>4</sub> powder in 5% H<sub>2</sub>/Ar. A small gain of mass (~0.17%) is observed between room temperature and 400 °C, implying that the mass gain probably comes from gas (hydrogen or argon) sorption. There is an abrupt weight loss between 400 and 900 °C, which is ascribed to the reduction of Mn<sup>4+</sup>/Mn<sup>3+</sup> to Mn<sup>3+</sup>/Mn<sup>2+</sup> and a lot of oxygen vacancies formed. The total weight loss in the range 20–900 °C is only 1.4 wt%. However, the reduced LSMO<sub>4</sub>

Table 1  
Structural parameters of LSMnO<sub>4</sub> synthesized at 1100 °C for 4 h from the XRD data.<sup>a</sup>

Atom	x	y	Z	Occupancy	$U_{iso}$ (Å <sup>2</sup> )
La	0	0	0.3556(2)	0.4	0.0087(3)
Sr	0	0	0.3556(2)	0.6	0.0087(3)
Mn	0	0	0	1	0.0075(0)
O(1)	0.5	0	0	1	0.0071(8)
O(2)	0	0	0.169	1	0.0083(8)

<sup>a</sup> Space group  $I4/mmm$  (139);  $a = b = 3.8173(3)$  Å;  $c = 12.3670(6)$  Å;  $V = 180.21$  Å<sup>3</sup>;  $R_{wp}$  (%) = 8.2;  $R_{exp}$  (%) = 10.1; the occupation of all atoms were fixed in the final refinement.

**Table 2**

Structural parameters of LSMO<sub>4</sub> after heating in 5% H<sub>2</sub>/Ar at 900 °C for 20 h from the XRD data.<sup>a</sup>

Atom	x	y	Z	Occupancy	U <sub>iso</sub> (Å <sup>2</sup> )
La	0	0	0.3591(5)	0.4	0.0069(5)
Sr	0	0	0.3591(5)	0.6	0.0069(5)
Mn	0	0	0	1	0.0101(4)
O(1)	0.5	0.0103(1)	0	1	0.0089(2)
O(2)	0	0	0.172	1	0.0125(2)

<sup>a</sup> Space group *I4/mmm* (139); *a* = *b* = 3.8805(3) Å; *c* = 12.7454(5) Å; *V* = 191.7 Å<sup>3</sup>; *R*<sub>wp</sub> (%) = 9.2; *R*<sub>exp</sub> (%) = 11.3; the occupation of all atoms were fixed in the final refinement.

**Table 3**

Electrical conductivity ( $\sigma$ ) and polarization resistance ( $R_p$ ) of LSMO<sub>4</sub> at various temperatures.

<i>T</i> (°C)	$\sigma$ (S cm <sup>-1</sup> )		$R_p$ (Ω cm <sup>2</sup> )	
	Air	5% H <sub>2</sub> (dry)	Air	5% H <sub>2</sub> (wet)
800	5.5	$0.4 \times 10^{-2}$	0.87	2.07
750	4.76	$0.2 \times 10^{-2}$	2.06	5.25
700	4.12	$0.1 \times 10^{-2}$	5.03	12.4

powder regained small weight on the cooling from 800 °C to 20 °C. This weight gain for LSMO<sub>4</sub> during cooling process may be attributed to the re-oxidation of Mn<sup>2+</sup>. In the overall TGA tested cycle, the total weight loss is about only 1.3 wt%, indicating that LSMO<sub>4</sub> is stable in 5% H<sub>2</sub>/Ar.

### 3.3. Morphology analyses

To observe any possible microstructure change after reduction, SEM images were taken from both as-prepared and reduced powders (Fig. 5), respectively. The powder is quite homogenous and the morphology of the powder did not change significantly after reduction. High-resolution transmission electron microscopy (HRTEM) of the pre-prepared and the reduced LSMO<sub>4</sub> samples showed in Fig. 6. It's found that a lattice spacing of 0.352 nm

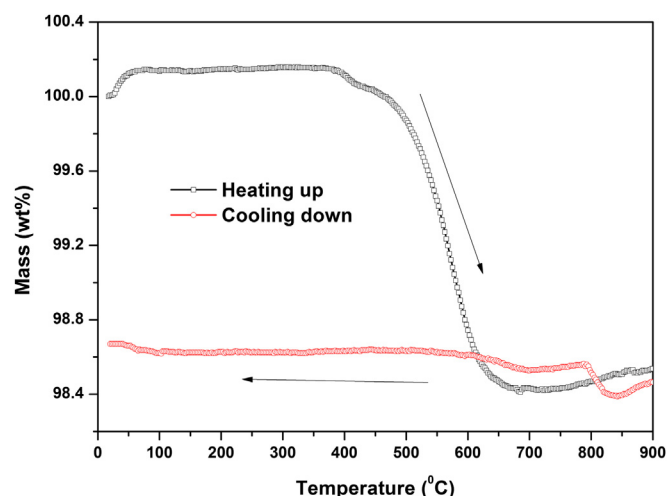


Fig. 4. TG experiments recorded during reduction of the pre-prepared samples of LSMO<sub>4</sub> in 5% H<sub>2</sub>/Ar.

(Fig. 6a) is agreement with the 0.359 nm separation between two (101) planes of the pre-prepared powder calculated from XRD pattern. However, a larger lattice spacing of 0.383 nm (Fig. 6b) can be obtained after LSMO<sub>4</sub> powder was reduced in 5% H<sub>2</sub> at 900 °C for 20 h. The value of lattice spacing is also consistent with that of 0.371 nm from XRD calculation for reduced sample. As showed in Fig. 6c, the results also confirm that a larger volume of unit cell is present.

### 3.4. Electronic conductivity analyses

Arrhenius plots for the electrical conductivity of LSMO<sub>4</sub> are showed in Fig. 7. Using a four-probe direct current measurement, the conductivities,  $\sigma$ , were measured in the temperature range of 300–800 °C in air and 5% H<sub>2</sub>, respectively. The electrical conductivities of LSMO<sub>4</sub> increased both in air and 5% H<sub>2</sub>, implying that LSMO<sub>4</sub> is a thermally activated semiconductivity which is due to the thermal promotion of electrons from donor levels or holes from acceptor levels [42]. At 800 °C, the  $\sigma$  value is 5.5 S cm<sup>-1</sup> in air, which is in agreement with previous works [19,43]. The conductivity of LSMO<sub>4</sub> is much higher in air than that in 5% H<sub>2</sub>/Ar. Meanwhile, the conductivity in 5% H<sub>2</sub> decreased dramatically to around  $0.4 \times 10^{-2}$  S cm<sup>-1</sup>, suggesting that electron holes were the main charge carries in LSMO<sub>4</sub>. The activation energy of conduction was calculated by the following equation:

$$\sigma = \frac{A}{T} \exp\left(\frac{-E_a}{kT}\right) \quad (1)$$

where *A* is the pre-exponential factor, *T* is the absolute temperature, *E<sub>a</sub>* represents the activation energy and *k* is the Boltzmann constant, respectively. As showed in Fig. 7, the calculated activation energy (0.110 eV) in air in this work is close with those reported by Skinner et al. [43]. However, a larger activation energy (1.395 eV) is observed in 5% H<sub>2</sub>.

The different behaviour of electronic conductivity under various atmospheres may involve the 3d orbitals of manganese. The layered perovskite manganite Sr<sub>2</sub>MnO<sub>4</sub> shows an antiferromagnetic insulating behaviour, having Mn<sup>4+</sup> ions with an electronic configuration of *t*<sub>2g</sub><sup>3</sup> [44]. When the Sr<sup>2+</sup> ions are partially replaced by La<sup>3+</sup> ions, *e<sub>g</sub>* electrons are doped into the system by the appearance of Mn<sup>3+</sup> ions with an electron configuration of *t*<sub>2g</sub><sup>3</sup> *e<sub>g</sub>*<sup>1</sup>. After reducing, Mn<sup>2+</sup> ions with an electron configuration *t*<sub>2g</sub><sup>3</sup> *e<sub>g</sub>*<sup>2</sup> are

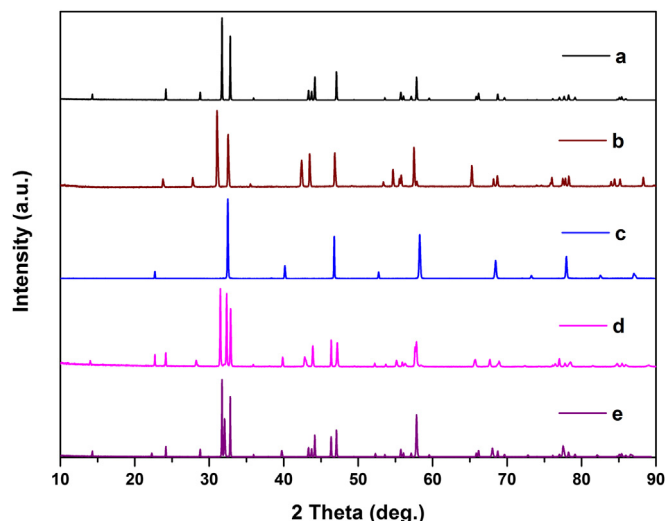


Fig. 3. XRD patterns of (a) LSMO<sub>4</sub> powders prepared at 1100 °C for 4 h, (b) LSMO<sub>4</sub> powders reduced in 5% H<sub>2</sub>/Ar at 900 °C for 20 h, (c) LSGM powders calcined at 1500 °C for 10 h, (d) LSMO<sub>4</sub>–LSGM mixtures after heating in air at 900 °C for 10 h, and (e) LSMO<sub>4</sub>–LSGM mixtures after heating in 5% H<sub>2</sub>/Ar at 900 °C for 10 h.

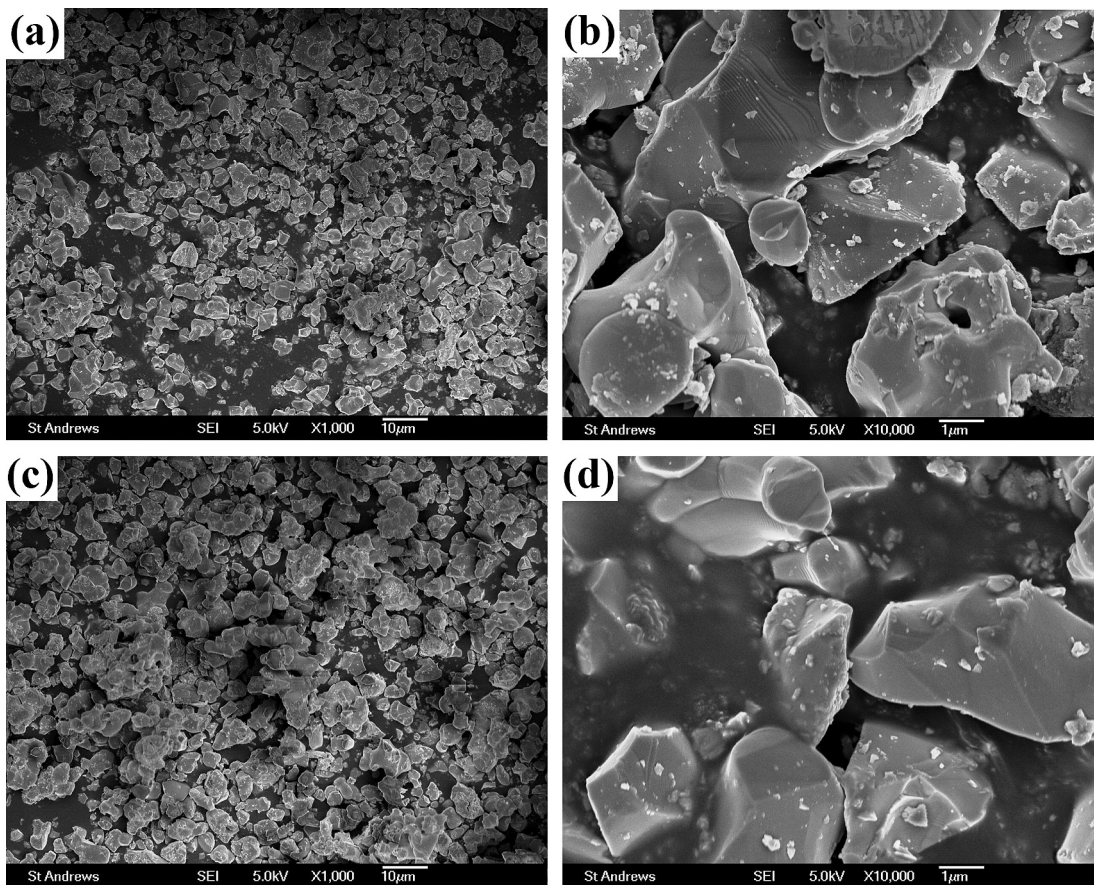


Fig. 5. SEM images of  $\text{LSMO}_4$  powder (a, b) before reduction and (c, d) after reduction at  $900^\circ\text{C}$  in  $5\% \text{H}_2$  for 20 h.

present. Here, we assume manganese is in a high spin state and neglect any Jahn–Teller splitting [45]. As described by Tuller [46], the  $3e_g$  orbitals of B-site cations in perovskite, e.g.  $\text{Mn}^{n+}$ , may overlap with the nearly  $2p_\sigma$  orbital from the split  $\text{O}_{2p}$  to form  $\sigma$ -bonds ( $e_g-p_\sigma-e_g$  bond), while the  $3t_{2g}$  orbital of manganese ions may overlap with the  $2p_\pi$  of  $\text{O}^{2-}$  ions to form weaker  $\pi$ -bonds ( $t_{2g}-p_\pi-t_{2g}$  bond). Although there is a third possibility of the direct  $t_{2g}-t_{2g}$  overlap for Mn d-orbital interactions, it is unlikely due to the large Mn–Mn distance across the face diagonal in perovskite-type structures [45]. It is assumed that electrons ( $e'$ ) or electron holes ( $h$ )

may hop from one Mn ion through the  $\sigma$  or  $\pi$ -bonds to a nearby Mn ion resulting in electronic conduction. The electronic conduction may have correlation with the  $e_g$  electron structure if the  $\sigma$ -bonds are the bridge.  $\text{LSMO}_4$  should exhibit low conductivity if the Mn valence is  $+2$  due to the low concentration of hole.

Thus, the larger ratio of  $\text{Mn}^{2+}$  ions in  $\text{LSMO}_4$ , the lower conductivity would be observed. On the other hand, it is reported that the electrical conduction would be dominated by the transition metal–oxygen–transition metal exchange interactions in the basal plane [47]. A loss in electron mobility and a drop in electrical conductivity

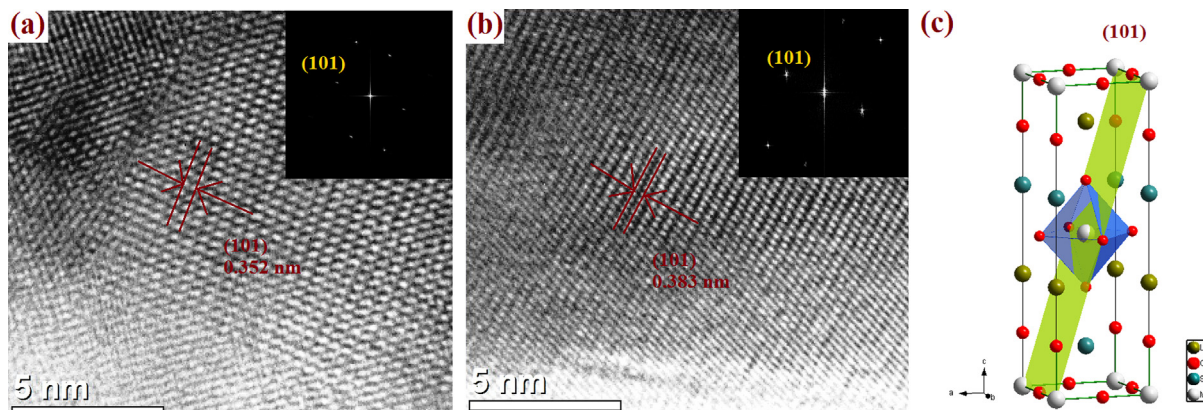


Fig. 6. TEM images of  $\text{LSMO}_4$  powder (a) before reduction, (b) after reduction, and (c) crystal structure with (101) plane.

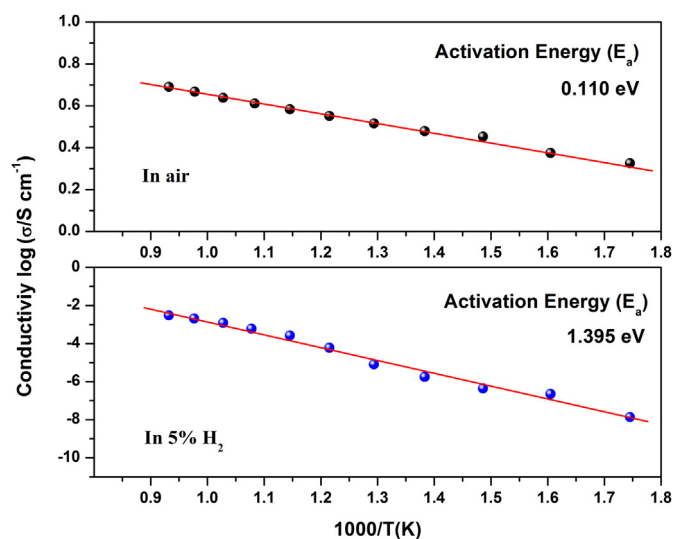


Fig. 7. Electrical conductivity of LSMO<sub>4</sub> in air and in 5% H<sub>2</sub> atmosphere at elevated temperatures.

would be present because of an increase of the inter-atomic distances within the *a/b* basal plane. From structural analysis, a larger volume caused by the increase of *a* and *c* was observed in LSMO<sub>4</sub> after reduction and thus obtained a lower electrical conductivity in 5% H<sub>2</sub>. Another consideration which may affect the electronic and ionic conductivities is the concentration of oxygen vacancies. The electrons main come from loss of lattice oxygen and formation of oxygen vacancies during the reducing process of manganese.

$$O_O^\times = V_O + \frac{1}{2} O_2(g) + 2e' \quad (2)$$

Water can form because the yield O<sub>2</sub> gas reacts with H<sub>2</sub> while created electrons may be trapped by manganese [44]. With increasing the concentration of oxygen vacancies, the 3D hopping path for electrons or holes through Mn–O–Mn may be blocked by oxygen vacancies leading to lower electron conductivity which is confirmed by our DFT + *U* calculations. The charge redistribution caused by an oxygen atom removal shows in Fig. 8. Compared with defect-free configuration, it obviously illustrates that Mn ions receive smaller electron density with an oxygen vacancy, because a

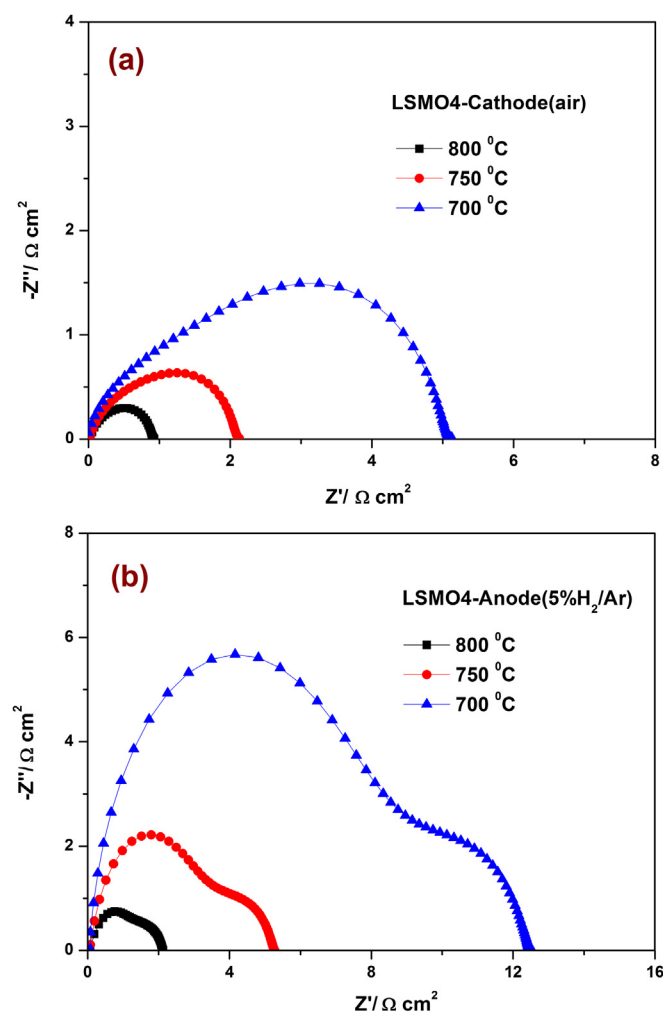


Fig. 9. Impedance spectra of the symmetrical half cell using LSMO<sub>4</sub> as electrodes measured (a) in air and (b) in 5% H<sub>2</sub>/Ar at 700, 750, and 800 °C, respectively. The electrolyte (LSGM) resistance has been subtracted from the cell impedance.

vacancy would attract the electron density close to that a missing ion [48]. Moreover, the Mn–O–Mn path is blocked by an oxygen vacancy. Especially, oxygen vacancies form along the Mn–O–Mn chains (Fig. 8c).

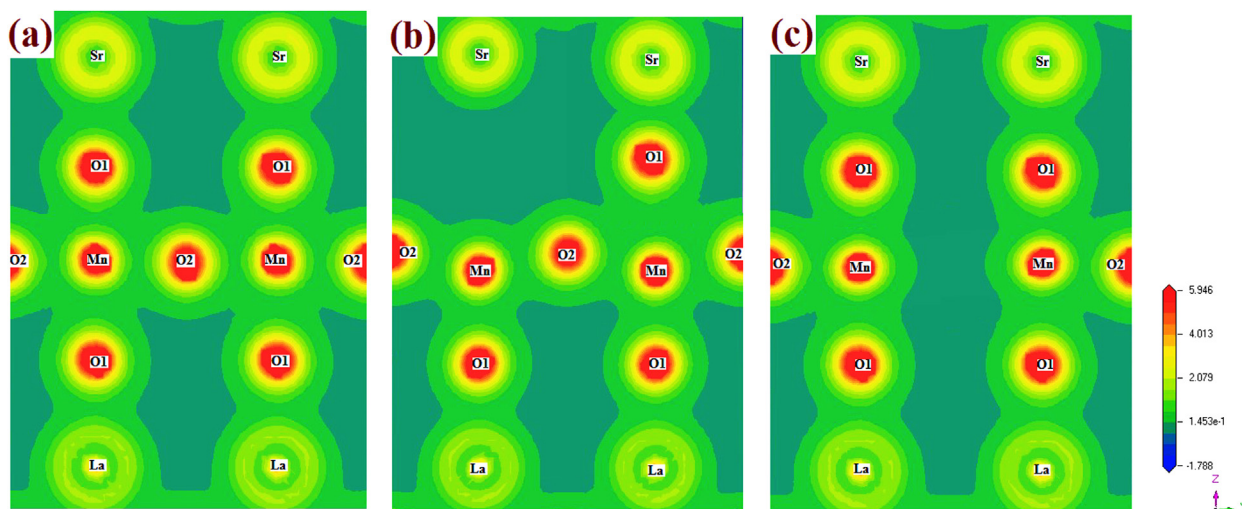


Fig. 8. The total electron densities in LSMO<sub>4</sub> (010) plane of (a) defect-free structure, (b) an oxygen vacancy along Sr–O–Mn path, and (c) an oxygen vacancy along Mn–O–Mn path.

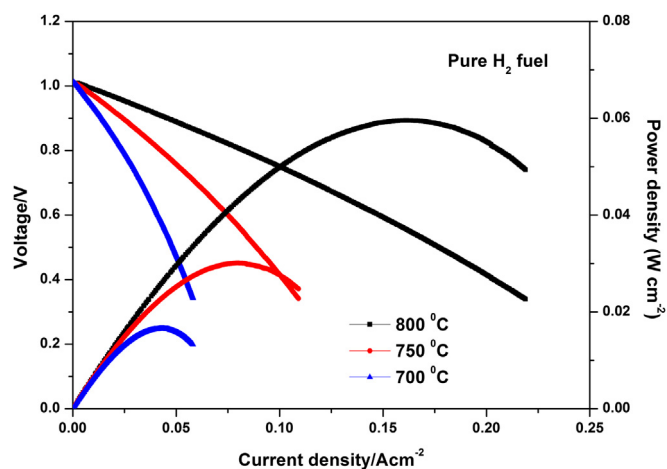


Fig. 10. Performance of a symmetrical fuel cell LSMO<sub>4</sub>|LSGM|LSMO<sub>4</sub> with pure H<sub>2</sub> as fuel.

### 3.5. Electrochemical properties and cell performances

Impedance spectroscopy measurements (Figs. 9a and b) were performed on the symmetrical LSMO<sub>4</sub>/LSGM/LSMO<sub>4</sub> cell over the temperature range 700–800 °C in air and under 5% H<sub>2</sub>, respectively. The LSMO<sub>4</sub> electrode polarization resistances in air were 0.87 Ω cm<sup>2</sup> at 800 °C, 2.06 Ω cm<sup>2</sup> at 750 °C, and 5.03 Ω cm<sup>2</sup> at 700 °C, respectively. The LSMO<sub>4</sub> electrode polarization resistances in 5% hydrogen were 2.07 Ω cm<sup>2</sup> at 800 °C, 5.25 Ω cm<sup>2</sup> at 750 °C, and

12.4 Ω cm<sup>2</sup> at 700 °C, respectively. The results imply that LSMO<sub>4</sub> exhibits better electrochemical activity for oxygen reduction than that for hydrogen oxidation. Fig. 10 shows the performance of a LSGM electrolyte-supported symmetrical fuel cell with the configuration of LSMO<sub>4</sub>/LSGM/LSMO<sub>4</sub> tested with pure wet H<sub>2</sub> as fuel. The thickness of the LSGM electrolyte is about 1.1 mm. The open circuit voltage (OCV) of the cell was 1.02 V at 800 °C using wet hydrogen, which is close to the value calculated from the Nernst equation. The maximum power density at 800 °C was 59 mW cm<sup>−2</sup>. The cross-section views of the LSMO<sub>4</sub>-based cell after operation are presented in Fig. 11. For both cathode and anode, good adherence between LSMO<sub>4</sub> and LSGM was observed with no cracks or delamination occurring at the interfaces. Moreover, the electrode displays a well-boned porous network and the particles are connected with each other, which is convenient for gas transporting to the activated sites.

## 4. Conclusions

The layered perovskite LSMO<sub>4</sub> was synthesized successfully by a citric-nitrate method. LSMO<sub>4</sub> has been investigated as prospective electrode material for IT-SSOFCs. Phase identification and morphology of LSMO<sub>4</sub> powder were determined by XRD, SEM and TEM before and after reduction. In a reducing atmosphere, it maintains the K<sub>2</sub>NiF<sub>4</sub>-type structure and a lattice expansion was observed. TGA performed in 5% H<sub>2</sub> indicates that the total weight loss is only 1.4 wt% range from 20 to 900 °C. The conductivities of LSMO<sub>4</sub> in air and 5% H<sub>2</sub> were 5.5 S cm<sup>−1</sup> and 0.4 × 10<sup>−2</sup> S cm<sup>−1</sup> at 800 °C, respectively. The lower conductivity in 5% H<sub>2</sub> and higher

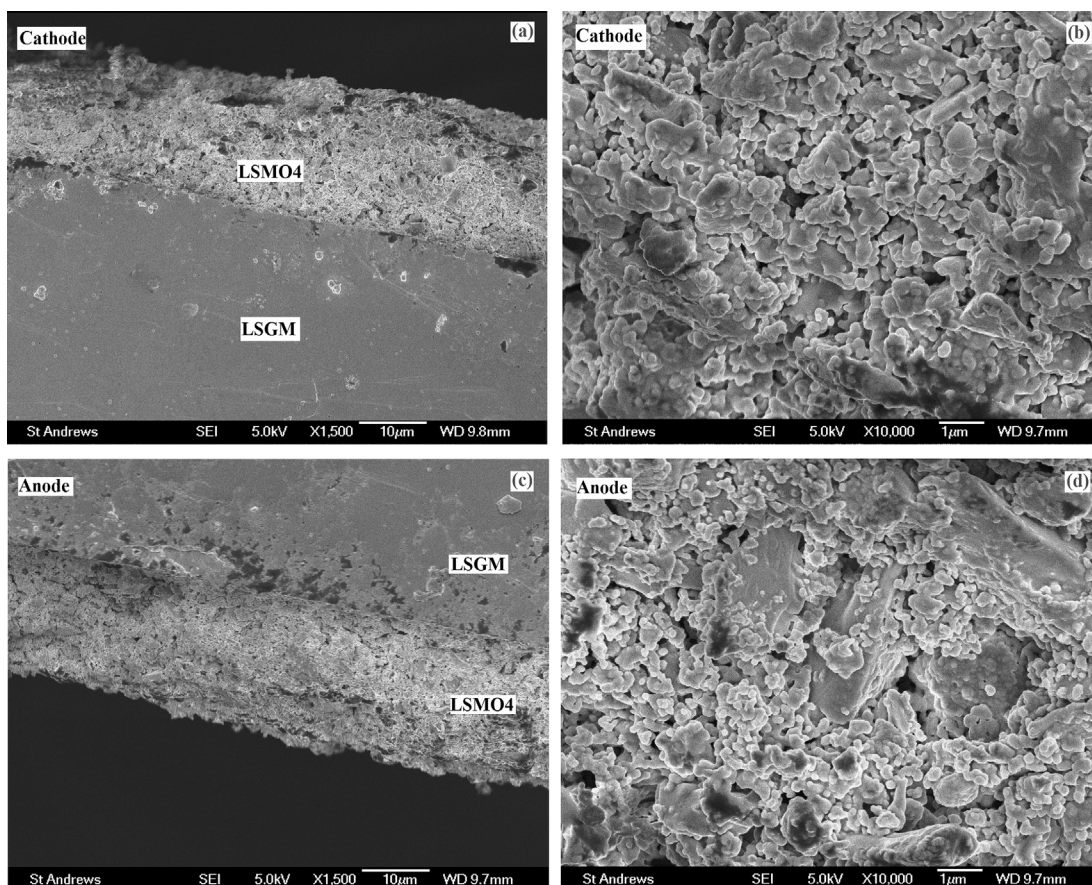


Fig. 11. SEM images of LSMO<sub>4</sub> operated as the cathode (a, b) and the anode (c, d) at 800 °C.

conduction activation energy than those in air would be caused by poorer overlap of both  $\sigma$  and  $\pi$  bonds due to the lattice expansion. DFT +  $U$  calculations show that oxygen vacancies which formed in reducing atmosphere may block the 3D hopping path for electrons or holes through Mn–O–Mn chains. At 800 °C, the polarization resistance of the LSMO<sub>4</sub> cathode is about 0.87  $\Omega$  cm<sup>2</sup> in air, while the polarization resistance of the LSMO<sub>4</sub> anode is about 2.07  $\Omega$  cm<sup>2</sup> in 5% H<sub>2</sub>. This shows that LSMO<sub>4</sub> can be applied as a cathode rather than an anode in conventional SOFC. Meanwhile, a better catalytic activity can be observed toward O<sub>2</sub> reduction than that of H<sub>2</sub> oxidation. A cell with LSGM electrolyte, LSMO<sub>4</sub>–LSGM mixture as anode and cathode simultaneously displays a maximum power density of 59 mW cm<sup>−2</sup> at 800 °C.

## Acknowledgements

Jun Zhou thanks Prof. John TS Irvine for his fruitful help and discussions. Jun Zhou also thanks the State Scholarship Fund of China Scholarship Council (No. 2011628082) for support.

## References

- [1] B.C.H. Steel, A. Heinzl, *Nature* 414 (2001) 345–352.
- [2] D.J.L. Brett, A. Atkinson, N.P. Brandon, S.J. Skinner, *Chem. Soc. Rev.* 37 (2008) 1568–1578.
- [3] N.P. Brandon, S. Skinner, B.C.H. Steel, *Rev. Mater. Sci.* 33 (2003) 183.
- [4] C. Xia, M.L. Liu, *Adv. Mater.* 14 (2002) 521.
- [5] A. Atkinson, S. Barnett, R.J. Gorte, J.T.S. Irvine, A.J. Mcevoy, M. Mogensen, S.C. Singhal, J. Vohs, *Nat. Mater.* 3 (2004) 17.
- [6] J.C. Ruiz-Morales, D. Marrero-Lopez, J. Canales-Vazquez, J.T.S. Irvine, *RSC Adv.* 1 (2011) 1403.
- [7] D.M. Bastidas, S. Tao, J.T.S. Irvine, *J. Mater. Chem.* 16 (2006) 1603.
- [8] J. Pena-Martinez, D. Marrero-Lopez, D. Perez-Coll, J.C. Ruiz-Morales, P. Nunez, *Electrochim. Acta* 52 (2007) 2950.
- [9] Y. Zhang, Q. Zhou, T. He, *J. Power Sources* 196 (2011) 76.
- [10] J.C. Ruiz-Morales, H. Lincke, D. Marrero-Lopez, J. Canales-Vazquez, P. Nun ez, *Bol. Soc. Esp. Ceram. Vidrio* 46 (2007) 218.
- [11] G. Kim, G. Corre, J.T.S. Irvine, J.M. Vohs, R.J. Gorte, *Electrochem. Solid State Lett.* 11 (2008) B16.
- [12] J.C. Ruiz-Morales, J. Canales-Vazquez, B. Ballesteros-Perez, J. Pena-Martinez, D. Marrero-Lopez, J.T.S. Irvine, P. Nun ez, *J. Eur. Ceram. Soc.* 27 (2007) 4223.
- [13] B. Lin, S. Wang, X. Liu, G. Meng, *J. Alloys Compd.* 490 (2010) 214.
- [14] Y. Zheng, C. Zhang, R. Ran, R. Cai, Z. Sao, D. Farrusseng, *Acta Mater.* 57 (2009) 1165.
- [15] A. El-Himri, D. Marrero-Lopez, J.C. Ruiz-Morales, J. Pena-Martinez, P. Nunez, *J. Power Sources* 188 (2009) 230.
- [16] Q. Liu, X. Dong, G. Xiao, F. Zhao, F. Chen, *Adv. Mater.* 22 (2010) 5478.
- [17] R. Sayers, J. Liu, B. Rustumji, S.J. Skinner, *Fuel Cells* 8 (2008) 338.
- [18] Y. Shen, H. Zhao, X. Liu, N. Xu, *Phys. Chem. Chem. Phys.* 12 (2010) 15124.
- [19] L. Sun, L. Huo, H. Zhao, Q. Li, P. Christophe, *J. Power Sources* 179 (2008) 96.
- [20] J. Zhou, G. Chen, K. Wu, Y.H. Cheng, *J. Phys. Chem. C* 117 (2013) 12991.
- [21] A. Tarancón, M. Burriel, J. Santiso, S.J. Skinner, J.A. Kilner, *J. Mater. Chem.* 20 (2010) 3799.
- [22] J. Zhou, G. Chen, K. Wu, Y.H. Cheng, *J. Power Sources* 232 (2013) 337.
- [23] C. Tealdi, C. Ferrara, P. Mustarelli, M.S. Islam, *J. Mater. Chem.* 22 (2012) 8969.
- [24] J. Zhou, G. Chen, K. Wu, Y. Cheng, B. Peng, J. Guo, Y. Jiang, *Appl. Surf. Sci.* 258 (2012) 3133.
- [25] A. Grimaud, F. Mauvy, J.M. Bassat, S. Fourcade, M. Marrony, J.C. Grenier, *J. Mater. Chem.* 22 (2012) 16017.
- [26] B. Peng, G. Chen, T. Wang, J. Zhou, J. Guo, Y. Cheng, K. Wu, *J. Power Sources* 201 (2012) 174.
- [27] S.J. Skinner, J.A. Kilner, *Ionics* 5 (1999) 171.
- [28] V.V. Kharton, A.V. Kovalevsky, M. Avdeev, E.V. Tsipis, M.V. Yaremchenko, E.N. Naumovich, J.R. Frade, *Chem. Mater.* 19 (2007) 2027.
- [29] M.A. Daroukh, V.V. Vashook, H. Ullmann, F. Tietzb, I. Arual Raj, *Solid State Ionics* 158 (2003) 141.
- [30] X. Ding, X. Kong, X. Wang, J. Jiang, C. Cui, *J. Alloys Compd.* 502 (2010) 472.
- [31] H. Zhao, Q. Li, L. Sun, *Sci. Chin. Chem.* 54 (2011) 898.
- [32] C. Jin, Z. Yang, H. Zheng, C. Yang, F. Chen, *Electrochem. Commun.* 14 (2012) 75.
- [33] A.C. Larson, R.B. Von-Dreele, *GSAS: General Structure Analysis System*, Los Alamos National Laboratory, Los Alamos, NM, 1994.
- [34] V. Milman, B. Winkler, J.A. White, C.J. Pickard, M.C. Payne, E.V. Akhmataskaya, R.H. Nobes, *Int. J. Quantum Chem.* 77 (2000) 895.
- [35] M.D. Segall, P.J.D. Lindan, M.J. Probert, C.J. Pickard, P.J. Hasnip, S.J. Clark, M.C. Payne, *J. Phys. Condens. Matter* 14 (2002) 2717.
- [36] J.P. Perdew, J.A. Chevary, S.H. Vosko, A.K. Jackson, R.M. Pederson, D.J. Singh, C. Fiollhais, *Phys. Rev. B* 46 (1992) 6671.
- [37] J.P. Perdew, Y. Wang, *Phys. Rev. B* 45 (1992) 13244.
- [38] D. Vanderbilt, *Phys. Rev. B* 41 (1990) 7892.
- [39] B.G. Prommer, M. Cote, S.G. Louie, M.L. Cohen, *J. Comput. Phys.* 131 (1997) 233.
- [40] S. Larochelle1, A. Mehta, L. Lu, P.K. Mang, O.P. Vajk, N. Kaneko, J.W. . Lynn, L. Zhou, M. Greven, *Phys. Rev. B* 71 (2005) 024435.
- [41] K. Rościszewski, A.M. Oleś, *J. Phys. Condens. Matter* 19 (2007) 186223.
- [42] J. Werner, M. Peisl, *Phys. Rev. B* 31 (1985) 6881.
- [43] C.N. Munnings, S.J. Skinner, G. Amow, P.S. Whitfield, I.J. Davidson, *Solid State Ionics* 177 (2006) 1849.
- [44] S. Larochelle, A. Mehta, N. Kaneko, P.K. Mang, A.F. Panchula, L. Zhou, J. Arthur, M. Greven, *Phys. Rev. Lett.* 87 (2001) 095502.
- [45] S. Tao, J.T.S. Irvine, *J. Mater. Chem.* 12 (2002) 2356.
- [46] H.L. Tuller, *Solid State Ionics* 94 (1997) 63.
- [47] G. Amow, P. Whitfield, I. Davidson, R.P. Hammond, C. Munnings, S. Skinner, *Solid State Chem. Mater. IV Boston* (2002) 347.
- [48] Y.A. Mastrikov, M.M. Kuklja, E.A. Kotomin, J. Maier, *Energy Environ. Sci.* 3 (2010) 1544.